Supporting Information

Redox Metal-Support Interaction of CoO_x/Ti_2O_3 to Enhance Catalytic Performance for Hydrodeoxygenation of Anisole

Weizhou Sun,[1] Masanori Nagao,[1,2] Miyu Sato,[1] Shuhei Shimoda,[3]

Yuichi Kamiya,[4] and Ryoichi Otomo[4, *]

[1]Graduate School of Environmental Science, Hokkaido University, Nishi 5 Kita 10, Kita-ku, Sapporo 060-0810, Japan. [2]National Institute of Technology, Tomakomai College, 443 Nishikioka, Tomakomai 059-1275, Japan. [3]Institute for Catalysis, Hokkaido University, Nishi 10 Kita 21, Kita-ku, Sapporo 001–0021, Japan. [4]Faculty of Environmental Earth Science, Hokkaido University, Nishi 5 Kita 10, Kita-ku, Sapporo 060-0810, Japan.

**Corresponding author: Dr. Ryoichi Otomo*

E-mail: otomo@ees.hokudai.ac.jp

Number of Pages: 19
Number of Tables: 3
Number of Figures: 14

Table S1 Composition (mol%) of synthesized Ti_2O_3 estimated by XRF.

Ti	Si	Nb	Cl	Zr	Total
99.66	0.16	0.14	0.03	0.01	100.00

Composition of the synthesized Ti_2O_3 was estimated X-ray fluorescence spectrometry using a Rigaku ZSX Primus III+ spectrometer. Si impurity derived from quartz wool that was used in the synthesis of Ti_2O_3. The other impurities derived from rutile TiO_2 that was the raw material for Ti_2O_3.

Table S2 Detailed results for hydrodeoxygenation of anisole over MoO_x/ZrO_2 at 250 – 350 ºC.

	250 °C	300 °C	350 °C
Anisole conversion (%)	5.3	15.6	61.3
Products yield (%)			
Benzene	0.0	4.3	23.2
Cyclohexane	0.0	0.0	0.0
Methoxycyclohexane	0.0	0.0	0.0
Phenol	0.0	2.2	5.9
Cresol	0.0	1.0	3.0
Toluene	0.0	1.4	11.0
Methylanisole	0.0	0.7	1.2
Dimethylanisole	0.0	0.0	0.6

Pretreatment conditions: H_2 flow (30 mL min^{-1}) at 250 – 350 ºC for 1 h. Reaction conditions: Catalyst, 0.20 g; Anisole, 0.020 mmol min^{-1}; Total flow rate (H_2 balance), 48 mL min^{-1}; Temperature, 250 – 350 ºC; Time on stream, 1 h.

Table S3 Summary of reported results for vapor-phase hydrodeoxygenation of anisole to benzene.

Catalysts	Temp. (°C)	P_{total} (MPa)	TOS (h)	Anisole Conv. (%)	Benzene Selec. (%)	STY [a] (mmol/g·h)	Ref.
10 wt% CoO_x/Ti_2O_3	250	0.10	1	69	79	3.2	This work
Mo_2C	150	0.10	0.28	7	82	3.6×10^{-2}	[1]
W_2C	150	0.13	0.28	4	98	1.0×10^{-2}	[1]
$NiMo/Al_2O_3$ [b]	250	1.50	n.d.	20	0	0	[2]
10 wt% Ni/Al_2O_3	270	0.50	24	69	60	1.1×10^{2}	[3]
3% Pt/UiO-66-def	270	1.00	3	86	52	1.2×10^{-2}	[4]
12 wt% CoNb/SBA-15 [c]	275	1.50	1	16	21	2×10^{-1}	[5]
20 wt% Ni/CeO_2	290	0.30	1	88	55	3.6	[6]
20 wt% Ni/TiO_2	290	0.30	1	51	74	2.8	[6]
20 wt% Ni/C	290	0.30	1	95	51	3.7	[6]
20 wt% Ni/SBA-15	290	0.30	1	99	82	6.1	[6]
20 wt% Ni/Al_2O_3	290	0.30	1	99	27	2.0	[6]
5 wt% Co/SBA-15	300	0.10	1	61	70	1.7	[7]
$Ni_{40}In/SiO_2$ [d]	300	0.10	n.d.	91	(60) [e]	2.0	[8]
10 wt% MoO_3/ZrO_2	320	0.10	4	50	20	7.3×10^{-1}	[9]
1 wt% Pt/SiO_2	375	0.10	0.25	15	7	3.0×10^{-3}	[10]
9 wt% Ru/SiO_2	375	0.10	0.25	5	16	1.0×10^{-2}	[10]
5 wt% Fe/SiO_2	375	0.10	0.25	8	85	1.0	[10]
1% Pt/SiO_2	400	0.10	0.5	100	69	1.6	[11]
15 wt% $Ni\text{-}Mo/SiO_2$	410	0.10	1	99	66	9.1	[12]
$Mo\text{-}Ni(OH)_2$	450	0.10	1	30	69	3.0	[13]

[a] Space-time yield of benzene; [b] 5 wt% Ni and 15 wt%; [c] 7.3 wt% Co and 4.7 wt% Nb; [d] 40 wt% Ni and Ni/In = 40; [e] Selectivity for BTX.

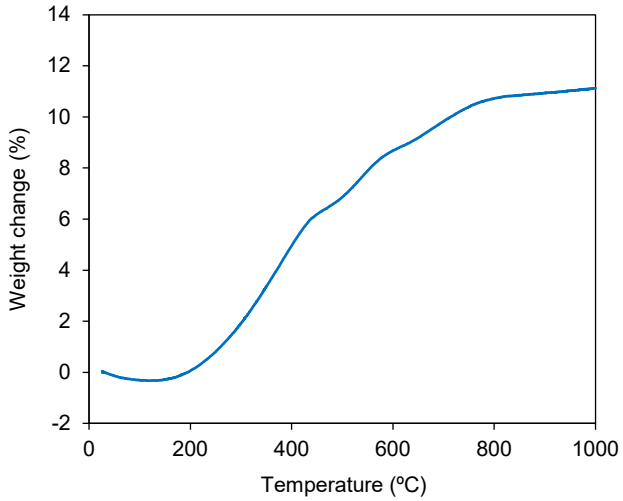

Figure S1 TG profile of synthesized Ti_2O_3.

TG profile was measured on synthesized Ti_2O_3 in air flow. After the temperature reached 1000 °C, Ti_2O_3 was completely oxidized to TiO_2. Based on weight gain due to the oxygen storage during this oxidation, the average valence of titanium for the original Ti_2O_3 was found to be 2.98, which was almost the same as the theoretical value of Ti_2O_3 (3.0).

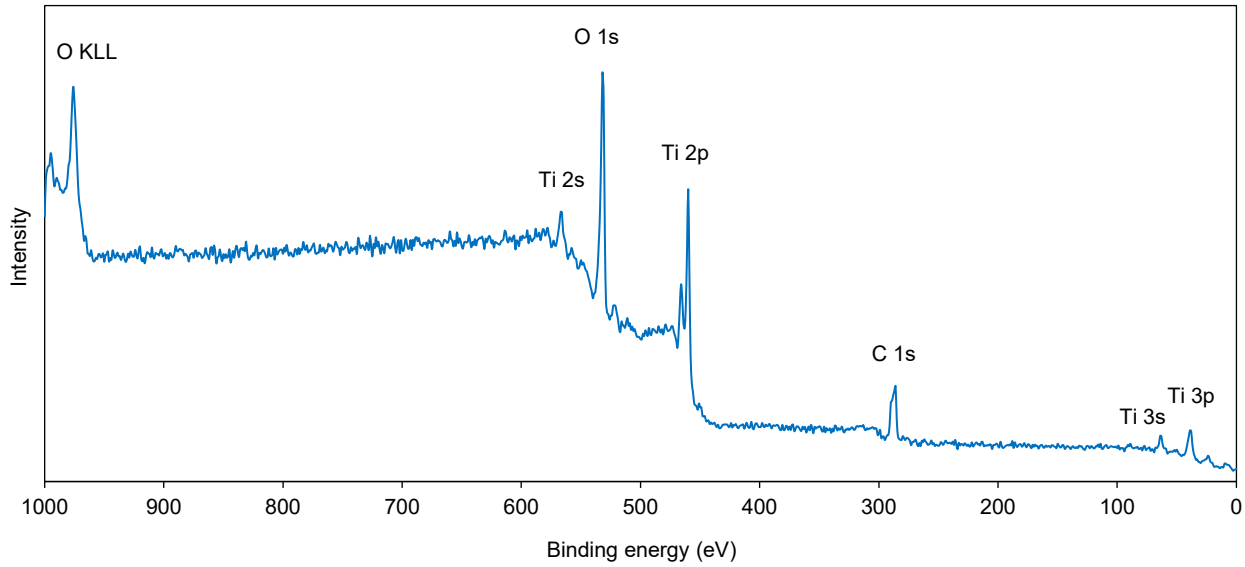

Figure S2 Wide-scan X-ray photoelectron spectrum of synthesized Ti_2O_3.

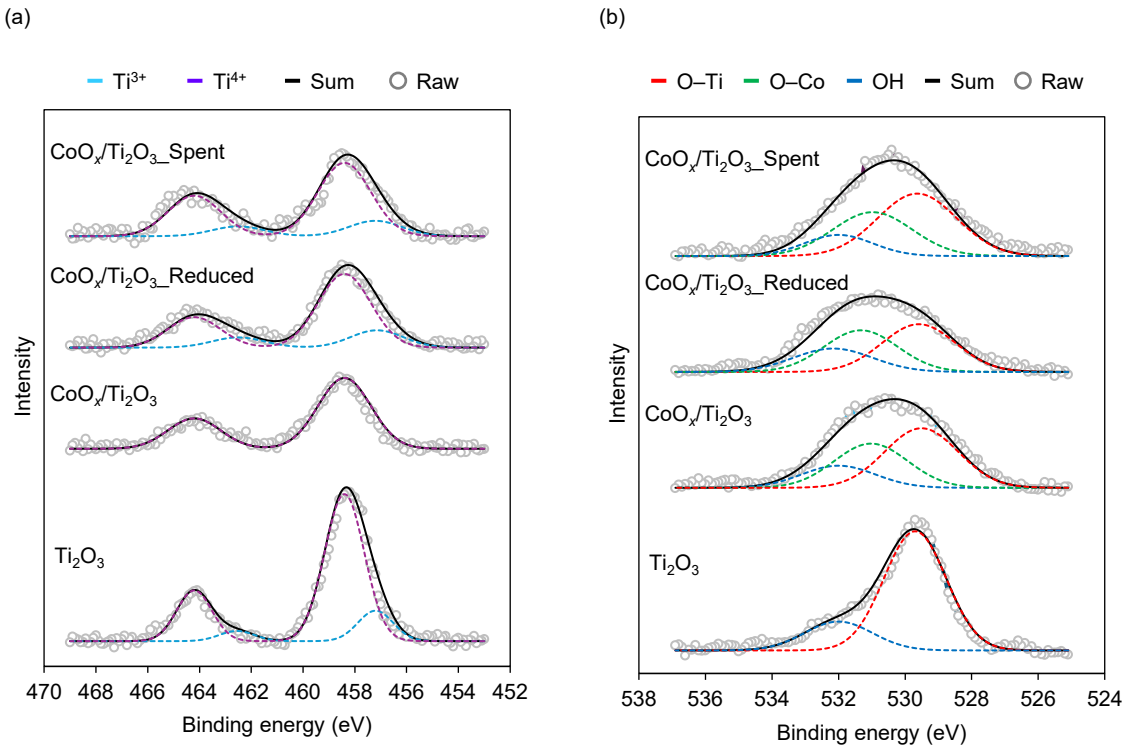

Figure S3 (a) Ti 2p and (b) O 1s X-ray photoelectron spectra of CoO_x/Ti_2O_3 samples. CoO_x/Ti_2O_3_Recuded and CoO_x/Ti_2O_3_Spent were CoO_x/Ti_2O_3 after treatment with H_2 at 250 ºC and after used in the HDO reaction shown in Figure 9, respectively.

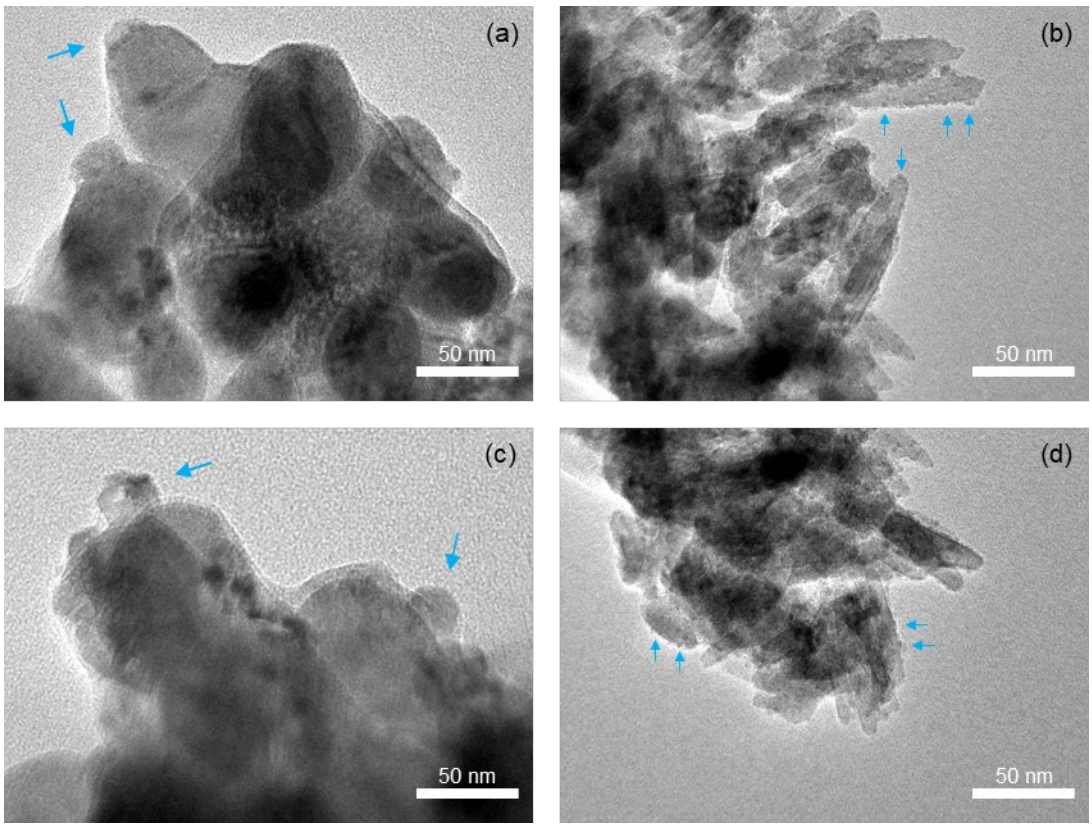

Figure S4 TEM images of (a) CoO_x/Ti_2O_3_Reduced, (b) CoO_x/TiO_2_Reduced, (c) CoO_x/Ti_2O_3_Spent, and (d) CoO_x/TiO_2_Spent.

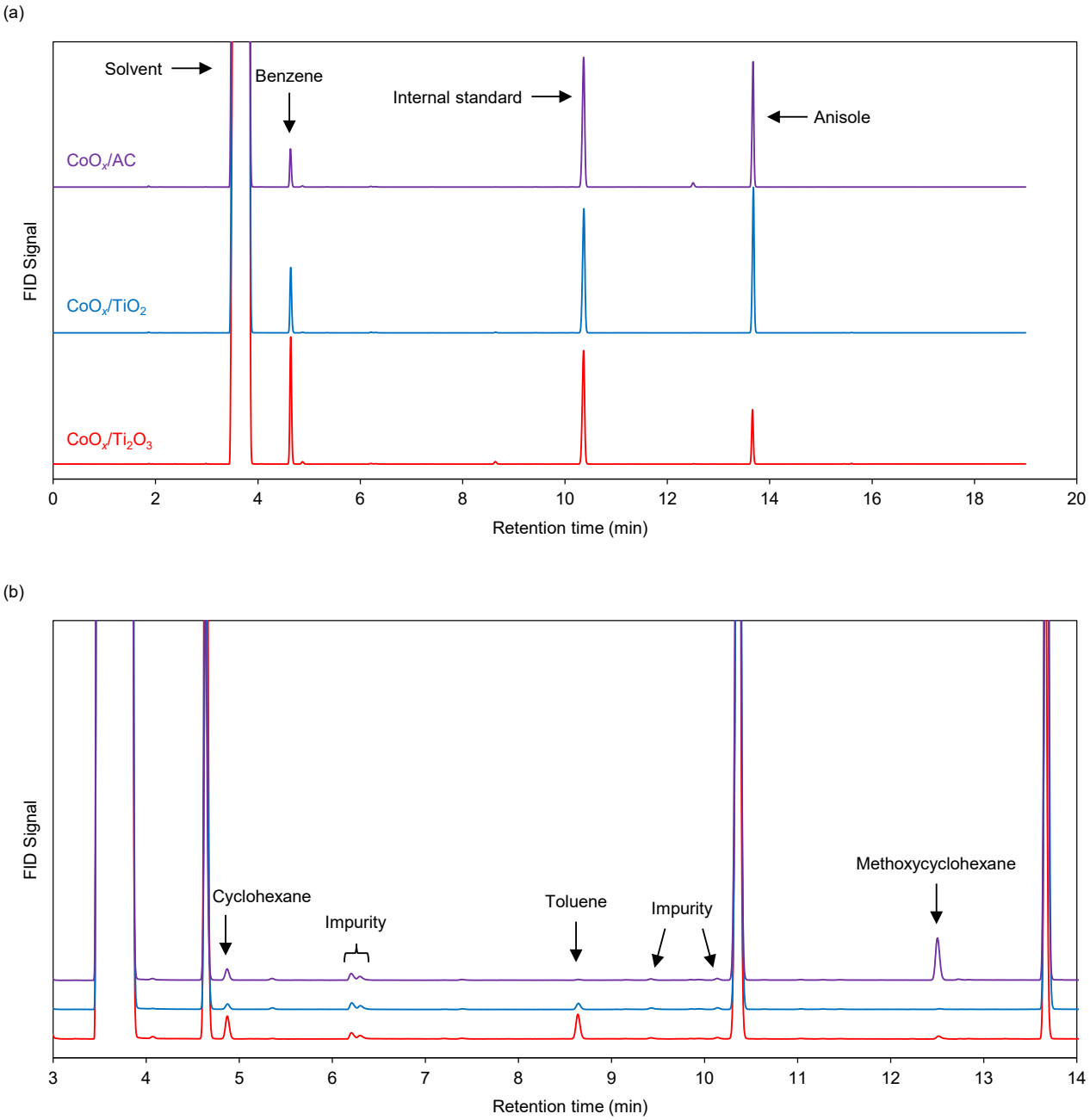

Figure S5 (a) Full and (b) Magnified chromatogram charts for HDO of anisole using CoO_x/Ti_2O_3, CoO_x/TiO_2, and CoO_x/AC shown in Figure 6.

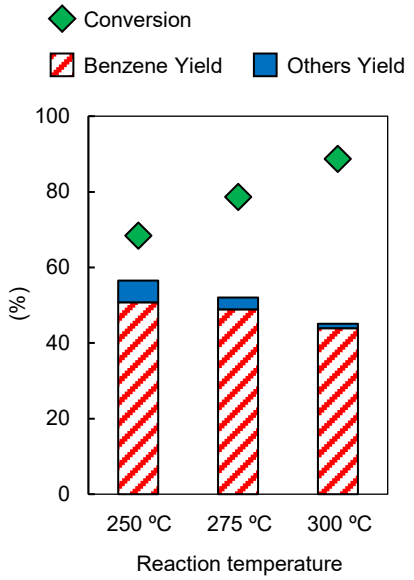

Figure S6 Influence of reaction temperature on HDO reaction of anisole over CoO_x/Ti_2O_3. Pretreatment conditions: H_2 flow (30 mL min^{-1}) at 300 ºC for 1 h. Reaction conditions: CoO_x/Ti_2O_3, 0.20 g; Anisole, 0.020 mmol min^{-1}; Total flow rate (H_2 balance), 48 mL min^{-1}; Temperature, 250 – 300 ºC; Time on stream, 1 h.

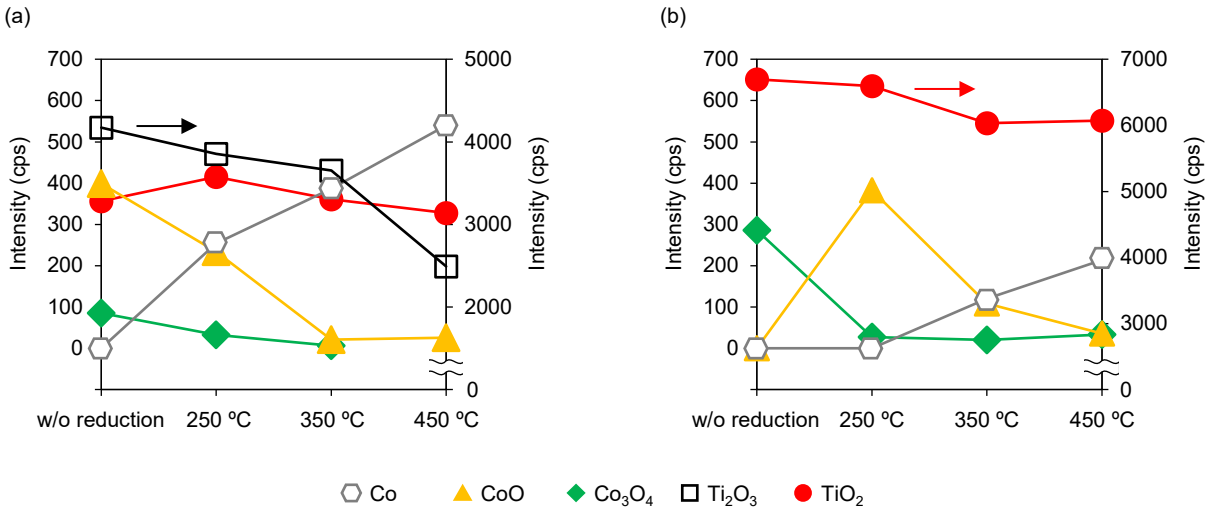

Figure S7 Variation curve for diffraction intensity of Co (2θ = 44.3°), CoO (2θ = 42.5°), Co_3O_4 (2θ = 31.3°), Ti_2O_3 (2θ = 23.9°), and TiO_2 (2θ = 27.5°) for (a) CoO_x/Ti_2O_3 and (b) CoO_x/TiO_2 after treatment with H_2 at 250 – 450 ºC.

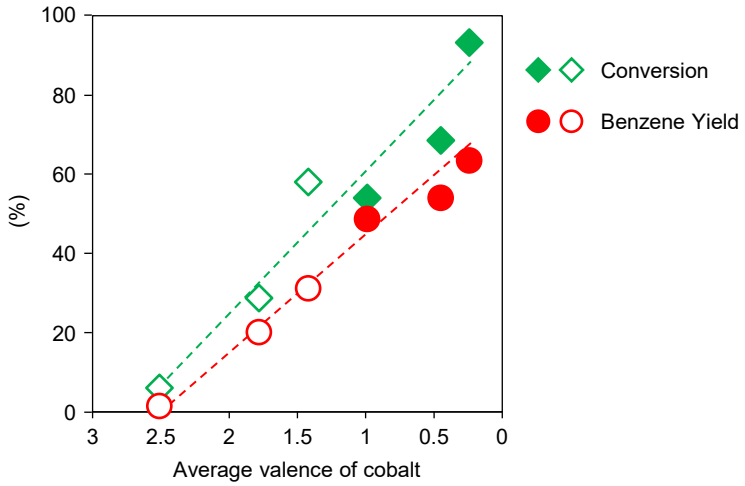

Figure S8 Relationship between catalytic activity and average valence of cobalt for CoO_x/Ti_2O_3 (filled symbol) and CoO_x/TiO_2 (blank symbol) catalysts pretreated at 250 and 350 ºC with H_2 or N_2. Pretreatment conditions: N_2 or H_2 flow (30 mL min^{-1}) at 250 – 450 ºC for 1 h. Reaction conditions: CoO_x/Ti_2O_3 or CoO_x/TiO_2, 0.20 g; Anisole, 0.20 mmol min^{-1}; Total flow rate (H_2 balance), 48 mL min-1^{-1}; Temperature, 250 ºC; TOS, 1 h.

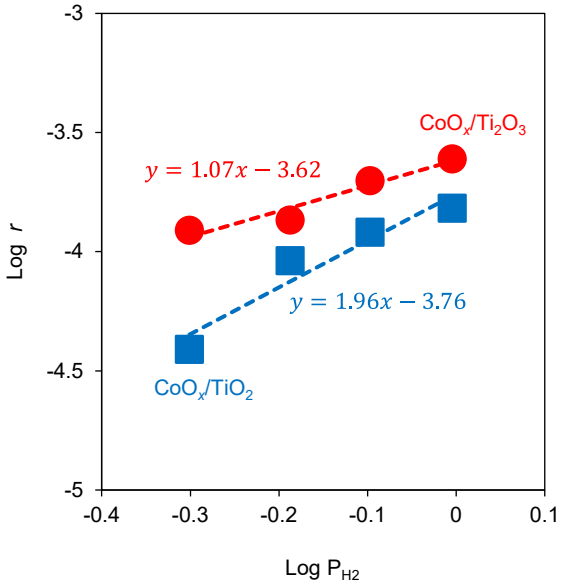

Figure S9 Hydrogen pressure dependance of reaction rate for HDO of anisole over CoO_x/Ti_2O_3 and CoO_x/TiO_2.

Pretreatment conditions: H_2 flow (30 mL min^{-1}) at 250 ºC for 1 h. Reaction conditions: CoO_x/Ti_2O_3, 0.20 g or CoO_x/TiO_2, 0.40 g; Anisole, 0.020 mmol min^{-1}; Total flow rate (N_2 balance), 48 mL min^{-1}; P_{H2}, 0.50, 0.65, 0.80, and 0.99 bar; Temperature, 250 ºC; Time on stream, 1 h.

To calculate formation rates of deoxygenated products (r), HDO reaction of anisole was conducted under different hydrogen pressures, and yield of the deoxygenated products was measured and calculate the formation rate r. Then, the relationship between the hydrogen partial pressure (P_{H2}) and the formation rate r was estimated according to the following equation, and the order of the hydrogen partial pressure was estimated.

$$r = k(P_{anisole})^a (P_{H2})^b$$
$$\Rightarrow \log r = b \log P_{H2} + a \log P_{anisole} + \log k$$

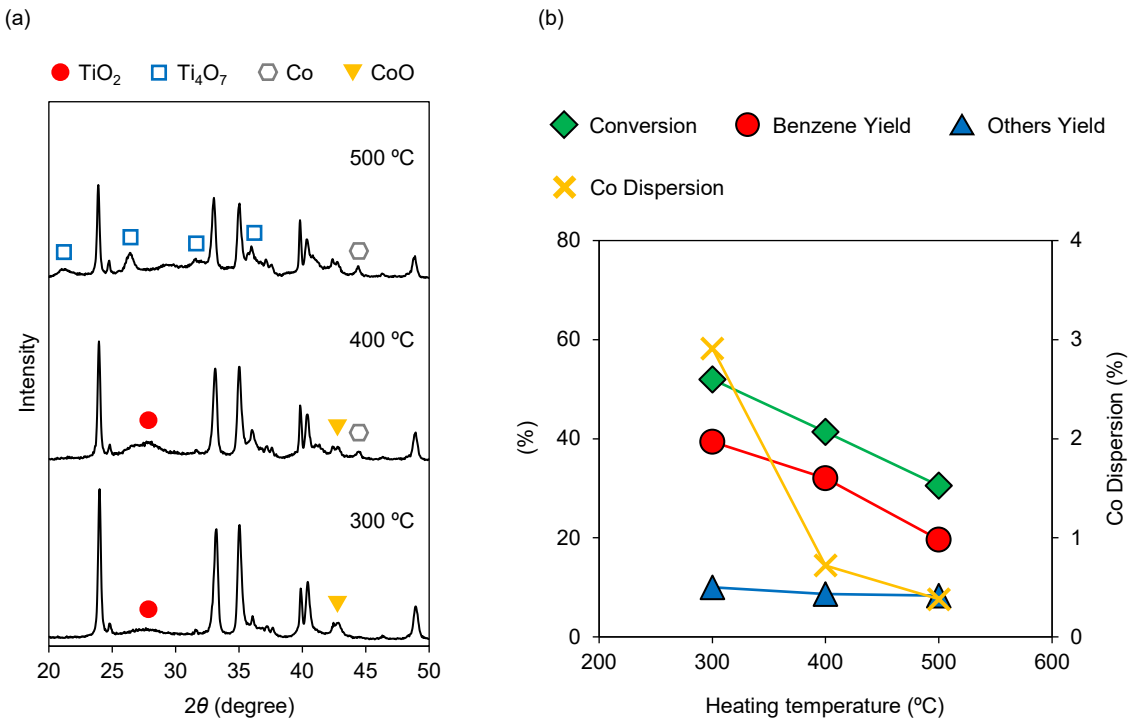

Figure S10 Influence of synthesis temperature on (a) structure and (b) catalytic performance of 5 wt% CoO_x/Ti_2O_3 for HDO of anisole.

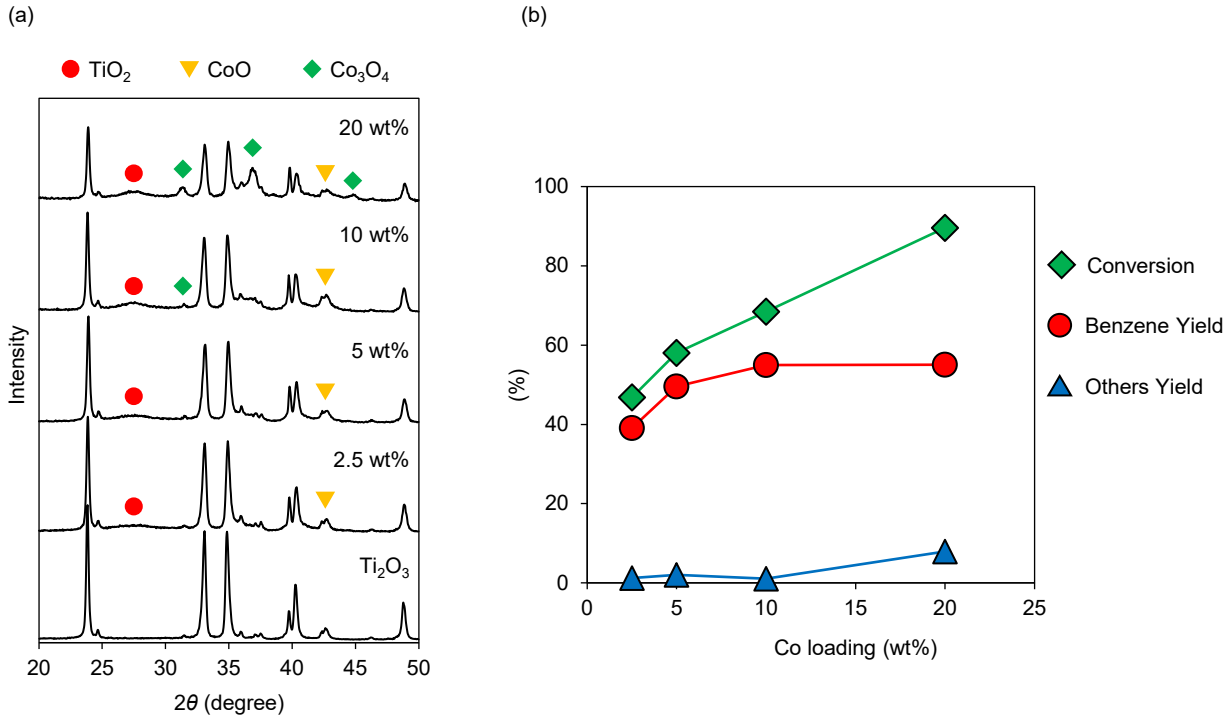

Figure S11 Influence of cobalt loading on (a) structure and (b) catalytic performance of CoO_x/Ti_2O_3 for HDO of anisole.

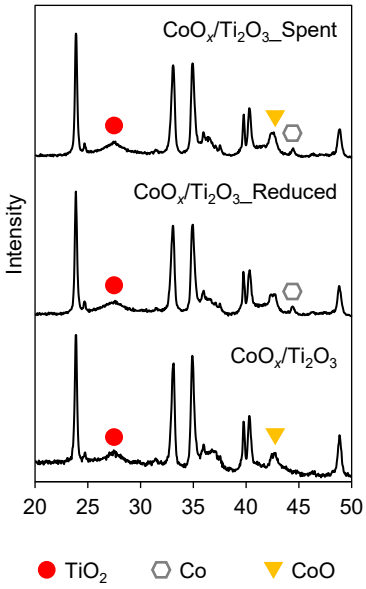

Figure S12 XRD patterns of CoO_x/Ti_2O_3 samples. CoO_x/Ti_2O_3_Recuded and CoO_x/Ti_2O_3_Spent were CoO_x/Ti_2O_3 after treatment with H_2 at 250 ºC and after used in the reaction shown in Figure 10, respectively.

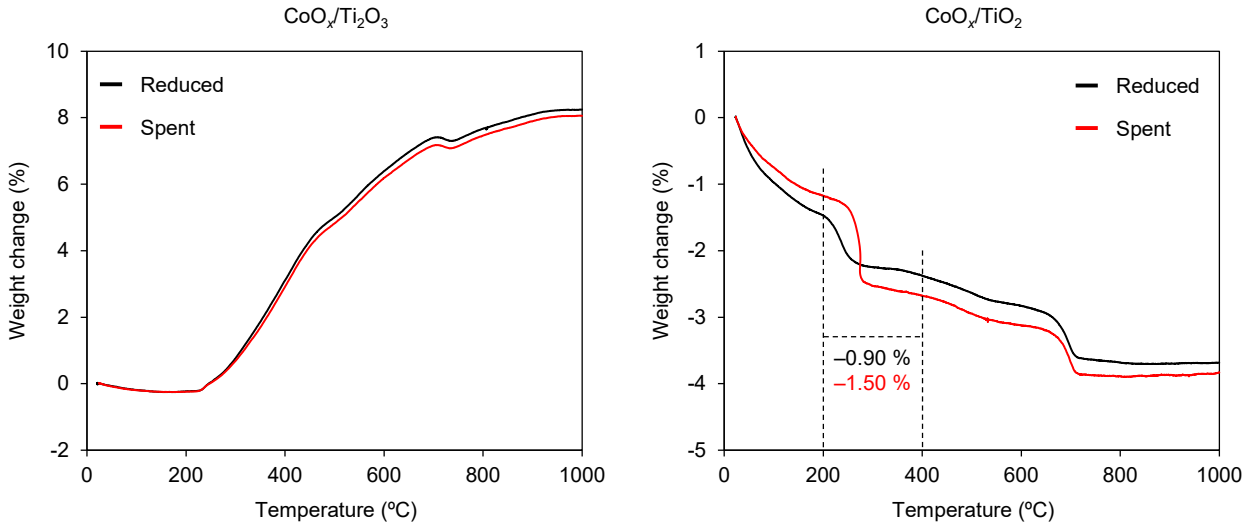

Figure S13 TG profiles of CoO_x/Ti_2O_3 and CoO_x/TiO_2 catalysts reduced with H_2 and used in the HDO reactions shown in Figure 10.

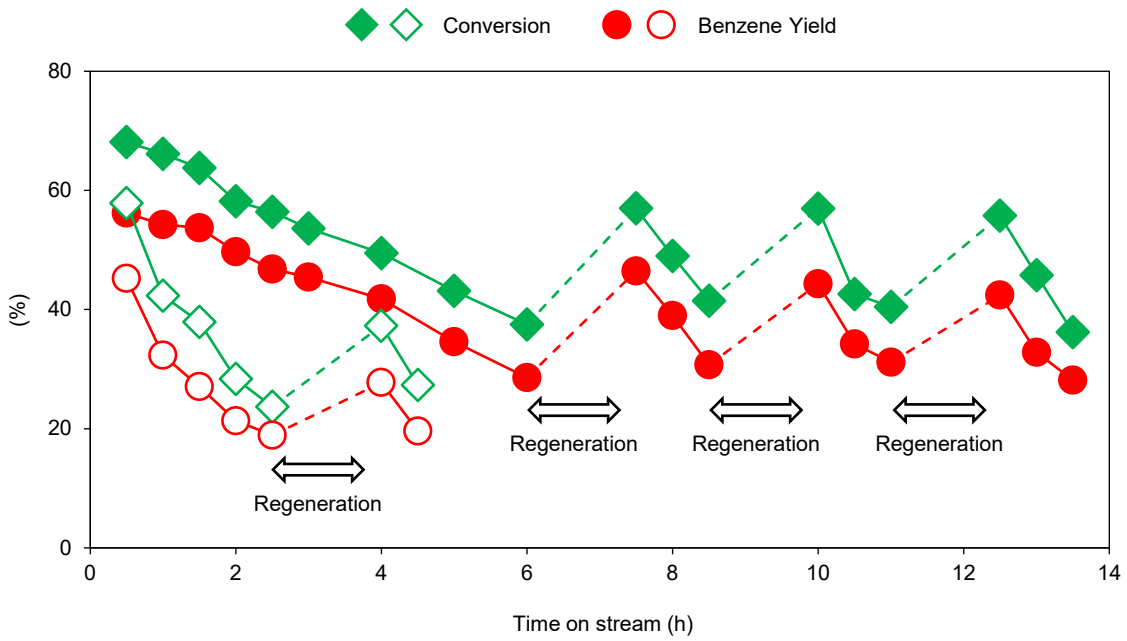

Figure S14 Regeneration of CoO_x/Ti_2O_3 (filled symbol) and CoO_x/TiO_2 (blank symbol) by treatment with H_2 in the middle of HDO of anisole.

Pretreatment and regeneration conditions: H_2 flow (30 mL min^{-1}) at 250 ºC for 1 h.

Reaction conditions: CoO_x/Ti_2O_3 or CoO_x/TiO_2, 0.20 g; Anisole, 0.020 mmol min^{-1}; Total flow rate (H_2 balance), 48 mL min^{-1}; Temperature, 250 ºC.

References

(1) Lu, Q.; Chen, C. J.; Luc, W.; Chen, J. G.; Bhan, A.; Jiao, F. Ordered Mesoporous Metal Carbides with Enhanced Anisole Hydrodeoxygenation Selectivity. *ACS Catal.* **2016**, *6* (6), 3506–3514. https://doi.org/10.1021/acscatal.6b00303.

(2) Hewer, T. L. R.; Souza, A. G. F.; Roseno, K. T. C.; Moreira, P. F.; Bonfim, R.; Alves, R. M. B.; Schmal, M. Influence of acid sites on the hydrodeoxygenation of anisole with metal supported on SBA-15 and SAPO-11. *Renew Energy* **2018**, *119*, 615–624. https://doi.org/10.1016/j.renene.2017.12.044.

(3) Dutta, S.; Shumeiko, B.; Aubrecht, J.; Karásková, K.; Fridrichová, D.; Pacultová, K.; Hlinčík, T.; Kubička, D. Evaluation of anisole hydrodeoxygenation reaction pathways over a Ni/Al_2O_3 catalyst. *Journal of Catalysis* **2024**, *435*. https://doi.org/10.1016/j.jcat.2024.115553.

(4) Phan, D. P.; Le, V. N.; Kim, J.; Lee, E. Y. Controlled hydrodeoxygenation of lignin-derived anisole over supported Pt on UiO-66 based-catalysts through defect engineering approach. *Fuel Processing Technology* **2021**, *224*. https://doi.org/10.1016/j.fuproc.2021.107001.

(5) Ballesteros-Plata, D.; Barroso-Martín, I.; Medina Cervantes, J. A.; Maciel, C.; Huirache-Acuña, R.; Rodríguez-Castellón, E.; Infantes-Molina, A. Bimetallic Niobium-Based Catalysts Supported on SBA-15 for Hydrodeoxygenation of Anisole. *Ind. Eng. Chem. Res.* **2021**, *60* (51), 18831–18840. https://doi.org/10.1021/acs.iecr.1c02799.

(6) Yang, Y.; Ochoa-Hernández, C.; de la Peña O'Shea, V. A.; Pizarro, P.; Coronado, J. M.; Serrano, D. P. Effect of metal–support interaction on the selective hydrodeoxygenation of anisole to aromatics over Ni-based catalysts. *Applied Catalysis B: Environmental* **2014**, *145*, 91–100. https://doi.org/10.1016/j.apcatb.2013.03.038.

(7) Yang, Y.; Lv, G.; Deng, L.; Lu, B.; Li, J.; Zhang, J.; Shi, J.; Du, S. Renewable aromatic production through hydrodeoxygenation of model bio-oil over mesoporous Ni/SBA-15 and Co/SBA-15. *Microporous and Mesoporous Materials* **2017**, *250*, 47–54. https://doi.org/10.1016/j.micromeso.2017.05.022.

(8) Wang, X.; Chen, J. Effects of indium on Ni/SiO_2 catalytic performance in hydrodeoxygenation of anisole as model bio-oil compound: Suppression of benzene ring hydrogenation and C–C bond hydrogenolysis. *Chinese Journal of Catalysis* **2017**, *38* (11), 1818–1830. https://doi.org/10.1016/S1872-2067(17)62910-3.

(9) Shetty, M.; Murugappan, K.; Green, W. H.; Román-Leshkov, Y. Structural Properties and Reactivity Trends of Molybdenum Oxide Catalysts Supported on Zirconia for the Hydrodeoxygenation of Anisole. *ACS Sustainable Chem. Eng.* **2017**, *5* (6), 5293–5301. https://doi.org/10.1021/acssuschemeng.7b00642.

(10) Tan, Q.; Wang, G.; Long, A.; Dinse, A.; Buda, C.; Shabaker, J.; Resasco, D. E. Mechanistic analysis of the role of metal oxophilicity in the hydrodeoxygenation of anisole. *Journal of Catalysis* **2017**, *347*, 102–115. https://doi.org/10.1016/j.jcat.2017.01.008.

(11) Zhu, X.; Lobban, L. L.; Mallinson, R. G.; Resasco, D. E. Bifunctional transalkylation and hydrodeoxygenation of anisole over a Pt/HBeta catalyst. *Journal of Catalysis* **2011**, *281* (1), 21–29. https://doi.org/10.1016/j.jcat.2011.03.030.

(12) He, T.; Liu, X.; Ge, Y.; Han, D.; Li, J.; Wang, Z.; Wu, J. Gas phase hydrodeoxygenation of anisole and guaiacol to aromatics with a high selectivity over $Ni\text{-}Mo/SiO_2$. *Catalysis Communications* **2017**, *102*, 127–130. https://doi.org/10.1016/j.catcom.2017.09.011.

(13) Aswin, P.; Narendranath, S. B.; Unni, A.; Balamurugan, S.; Venkatesha, J.; Sakthivel, A. Molybdate

incorporated α-$Ni(OH)_2$: potential catalyst for oxidation of Iso-eugenol and anisole hydrotreating. *Journal of Chemical Sciences.* **2023**, *135*, 99. https://doi.org/10.1007/s12039-023-02218-6.